CHALMERS

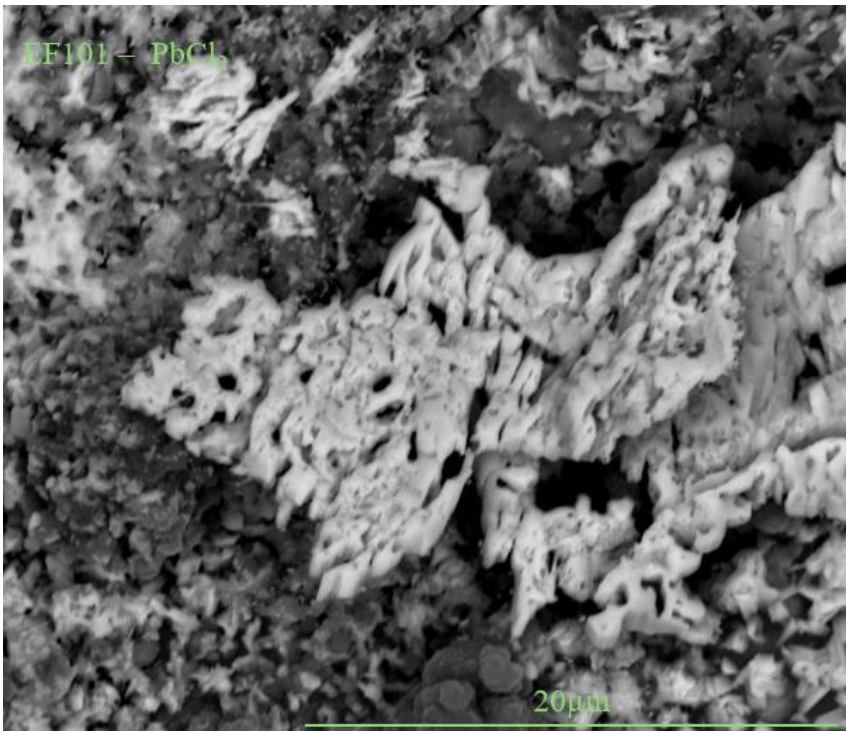

A Corrosion Study on a Novel FeCrAl Alloy for Water Wall Applications in Waste-Fired Boilers

Bachelor's thesis in Chemical Engineering

JOACHIM RÖDBRO

DEPARTMENT OF CHEMISTRY AND CHEMICAL ENGINEERING

CHALMERS TEKNISKA HÖGSKOLA
Göteborg, Sverige 2024
www.chalmers.se

DEPARTMENT OF CHEMISTRY AND
CHEMICAL ENGEENERING
CHALMERS TEKNISKA HÖGSKOLA
Göteborg, Sverige 2024
www.chalmers.se

BACHELOR'S THESIS 2024

A Corrosion Study on a Novel FeCrAl Alloy for Water Wall Applications in Waste-Fired Boilers

JOACHIM RÖDBRO

CHALMERS

Department of Chemistry and Chemical Engineering
Division of Energy and Materials
Chalmers University of Technology
Gothenburg, Sweden 2024

© JOACHIM RÖDBRO, 2024.

Supervisor: Hampus Lindmark, PhD student, Department of Chemistry and Chemical Engineering
Examiner: Jesper Liske, Associate Professor, Department of Chemistry and Chemical Engineering

Bachelor's Thesis 2024
Department of Chemistry and Chemical Engineering
Division of Energy and Materials
Chalmers University of Technology
SE- 412 96 Gothenburg
Telephone +46 735 099 460

Cover: Image of oxide formation from a FeCrAl alloy sample exposed to $PbCl_2$ and 400 °C for 168 hours. Image is taken with SEM instrument and has a magnification of 8000x.

Gothenburg, Sweden 2024

Abstract

Today, as society faces greater challenges regarding waste handling, the European commission have putting out directives for waste handling called “waste hierarchy”. This includes converting waste to energy. There are several technologies available of which one is the so called CFB boiler, Circulating Fluidized Bed Boiler. In this boiler the waste fuel is combusted and the heat in the flue gas is used to heat water into steam inside heat exchangers. The steam can generate electricity via a steam turbine and the heat can be used in a district heating net. The heat exchangers, e.g., superheater tubes and water walls, inside the boiler is made of metallic components. One problem a CFB boiler is facing is that the water wall heat exchangers get exposed to both heavy metals and chlorine originating from the waste. This accelerates the corrosion rate of the water wall materials. The material is usually of low-alloyed steel and a method for increasing the corrosion resistance is to put a layer of Ni-based alloy on top of the material, a so called coating. However, because of the high cost of the Ni-based coating other cheaper materials are currently under consideration. One of these is Kanthal EF101. The aim for thesis is to evaluate the corrosion rate for Kanthal EF101 when exposed to two heavy metal compounds, PbO or $PbCl_2$ and compare it with a Ni-based alloy (Alloy625) and low-alloyed steel (T22). For this, multiple factors must be considered for example thermodynamics, kinetics, the principles of oxide formation and influence of PbO and $PbCl_2$. The experiments in this project were divided into three steps; sample preparation, exposure and analysis. All exposures were performed with a laboratory environment simulating the water-wall in a waste fired boiler and lasted for 168 hours. The analysis used SEM and EDX instruments to create backscattered images for classification of elements on the sample and investigate the oxide growth. The results showed that EF101 has similar good protection properties as the Ni-based alloy Alloy625 and much greater protection than the low-alloyed steel T22. The presence of chlorine increased the corrosion rate of the samples, as the samples exposed to $PbCl_2$ was severely more corroded than the corresponding samples exposed to PbO.

Acknowledgment

I would like to express my deepest appreciation for everyone who supported me and made this project possible. This has been a great opportunity for me to grow, both academically, in the laboratory as well as personally.

First and foremost, I would like to thank my examiner Associate Professor Jesper Liske for his encouragement and insightful feedback and for giving me the opportunity to pursue this project.

I am tremendously grateful for my supervisor, Ph. D Hampus Lindmark for his continuous support, guidance and patience throughout my thesis. I'm immensely thankful for your expertise, pedagogical discussion and engagement for my growth and for your help with my thesis.

Specially thanks to my two office mates, Igor Mitrovic and Petter Jacobsson for the various discussions, support, helpfulness and laughter we shared. I have not only learned a lot from you two, but your friendship has also made this experience profoundly delightful.

Finally, I wanted to take a moment to extend my heartful thanks to my family – my mom, dad and sister– for your unconditional love and continuous support. You have always been there for me and for that I'm forever grateful.

With heartfelt appreciation,
Joachim Rödbro

Acronyms

CFB – Circulating fluidized bed boiler

WtE – Waste to energy

HTC – High temperature corrosion

SEM – Scanning electron microscopy

BSE – Backscattered electrons

SE – Secondary electrons

EDX – Energy dispersive X-ray

BIB – Broad ion beam

Contents

1.Introduction

1.1 Background

Today, society faces great challenges regarding waste handling. As the global population and economy grows, so does the amount of waste. Today, a cheap and common way of handling waste, is to dispose of it in landfills [1]. However, this approach may contribute to many environmental and health problems as waste decomposition over time may lead to release of toxins that could contaminate the surrounding environment. Furthermore, reports have shown that uncontrolled combustion may occur in landfills [1]. This may lead to emission of methane, a greenhouse gas 28 more potent that CO_2 [2]. As an approach to mitigate the volume of landfills, the European commission have established a certain priority for waste handling, the so-called waste hierarchy. When prevention, reuse or recycling is not an option, recovery of waste in form of electricity and heat should be established by the so-called waste-to-energy (WtE) technology [3].

WtE does not only play a key role for reducing landfill volumes, but also in producing renewable electricity and heat. When large fraction of waste contains biomass, such as branches from the forest industry, recycled wood waste from the furniture industry, or sawdust from the sawmill, substitution of fossil fuel with waste becomes a great renewable energy source. In Sweden, WtE is well established and provides thousands of households with renewable electricity and district heating. One process using WtE technology is fluidized bed boilers used for combustion of waste in combined heat and power plants (CHP) [3].

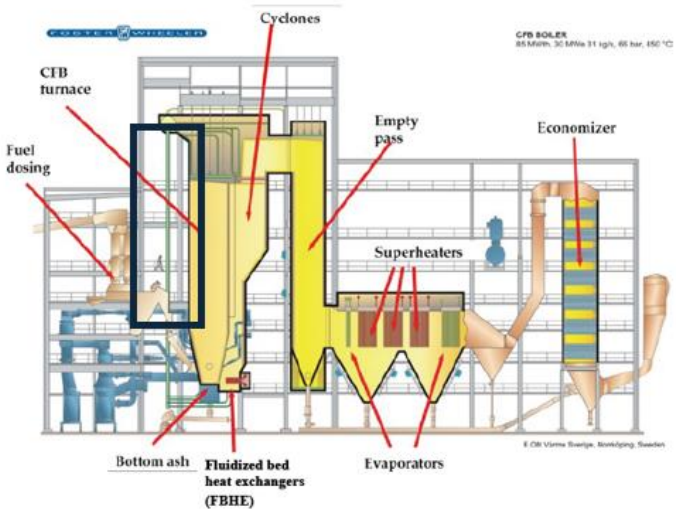

Figure 1.1: Schematic of a circulating fluidized bed combustion [3]

Figure 1 illustrates a circulating fluidized bed CFB boiler were waste converts into electricity and heat [3]. The fuel is introduced to the boiler in the so-called fuel dosing area and transported to the furnace chamber. Air is blown at the bottom of the furnace chamber to promote complete combustion. A fluidized bed material, such as quartz, is also introduced to the furnace chamber to promote a more homogenous combustion. The produced flue gas travels to the cyclone where it is separated from the fluidized bed material via gravitational and centrifugal forces. The flue gas continuous traveling to the convective superheaters where heats up saturated steam to superheater steam. The superheated steam is then transported to a turbine where the thermal energy is converted to kinetic energy which is used to rotate a turbine and subsequently used to generate electricity via a generator. The superheated steam is then cooled down and recirculates to the water wall region. The hot flue gas heats the water wall tubes, producing saturated steam. The gas is then transported to the top of the water-wall region and eventually transported to the superheaters. Generally, the material facing the fireside of a water wall tube has a temperature between 300-400 °C [3].

Today, one severe problem among others remains with CHP plants and it is the presence of heavy metals, such as PbO and $PbCl_2$. This is because of lead which are highly reactive element and originates from different materials in the waste. One other element that is also highly reactive in these enivirоment is chlorine. These compounds produce a highly corrosive flue gas originating from the biomass and waste fuel. Usually, the water wall consists of a low-alloyed steel due to it having a low cost and good mechanical properties. However, in these corrosive

environments the low-alloyed steel significantly reduces its performance lifespan due to its lack of protection against corrosion [4]. To combat the high corrosion rate, Ni-based alloy is commonly coated over the low-alloyed steel. The Ni-based alloy has a remarkable good corrosion resistance due to the alloy's amount of nickel and chromium [5]. The chromium produces a protective and stable oxide called chromia (Cr_2O_3). The main problem with Ni-based alloys is the high cost since it contains high amount of nickel and therefore other cheaper material options is constantly being researched for applying it in waste-boilers applications as well [4,5].

An alloy type that has a potential to replace Ni-based alloys for water wall application is FeCrAl alloys, called Kanthal EF101 [3]. This alloy has been mostly used in temperatures between 900-1300 °C, where it produces a highly protective alumina-based oxide, called α-Al_2O_3. Unfortunately, this oxide has a low formation rate due to it being unstable in lower temperatures. However, previous studies indicates that by increasing the amount of Si, Al and Cr the protection properties improve against corrosion [3,6]. FeCrAl is also an iron-based metal, making it a more affordable material than the Ni-based alloy [5,6].

By this the FeCrAl alloy seems to have the right properties to compete against the Ni-based alloy. Unfortunately, the studies for FeCrAl at temperatures relevant for water wall application (400 °C) is limited and therefore it is highly important to increase the knowledge surrounding this alloy at water-wall applications for CFBs [3].

1.2 Aim

The aim of this thesis is to evaluate the corrosion rate of a newly developed FeCrAl alloy, called Kanthal EF101, when exposed to a combination of either PbO or $PbCl_2$ in an environment simulating that of the water walls region of waste-fired boilers. Furthermore, this thesis will evaluate the corrosion rate of FeCrAl alloy and compare it with the more conventional Ni-based alloy 625 and a low-alloyed steel reference, named T22.

1.3 Limitations

Due to limited time the primary focus will be to analyse the extent of the corrosion attack on the alloy types and to compare the corrosion attack against the Ni-based and low-alloyed steel using advanced scanning electron microscopy.

2.Theory

High temperature corrosion (HTC) is the degradation and oxidation of metals under high temperature [7]. Generally, HTC occurs in oxidizing environment as for example, in industrial processes were oxygen or other commonly corroding gases are present. [7].

2.1 Thermodynamics for HTC

What kind of oxide that forms on metals depends on their alloy composition and can be predicted by thermodynamics. This is accomplished by predicting both temperature and specific environmental conditions using the following equations [8].

$$\Delta G = \Delta H - T\Delta S \qquad (2.3)$$

Equation 2.3 above is showing the equation of the Gibbs free energy, where G is Gibbs free energy, H is enthalpy, S is entropy and T is temperature. The equation can primarily influence the state of stability of either metal or the oxide wherever the pressure or temperature is constant. If $\Delta G < 0$, a reaction is spontaneous and if $\Delta G > 0$, the reaction needs external input of energy to take place. Lastly if the $\Delta G = 0$, the reaction has reached an equilibrium [8].

$$\Delta G = \Delta G° + RTln\frac{a_{M_aO_b(s)}}{a^a_{M(s)}a^{\frac{b}{2}}_{O_2(g)}} \qquad (2.4)$$

Equation 2.4 demonstrates The Gibb free energy equation for metals and oxides, where M_aO_b is the oxide, a is the chemical activity of the reactants and products, R and T are ideal gas constant and temperature and $\Delta G°$ is the standard free energy change. In most cases, the activity of gases is estimated to be the same as the partial pressure. The activity of pure solids is commonly 1. When the partial pressure of oxygen $p(O_2)$ is equal to the activity of the gas compound, the equation can be rewritten like this [8]:

$$\Delta G° = RTln(P_{O_2}) \qquad (2.5)$$

Where both the metal and the oxide product are in a solid state, and if metal and oxide are both at equilibrium with each other, the oxide is incapable of being formed [8].

The Ellingham diagram below is a graphical representation for differences of the standard Gibbs free energy of oxidation as a function of the oxygen partial pressure [9].

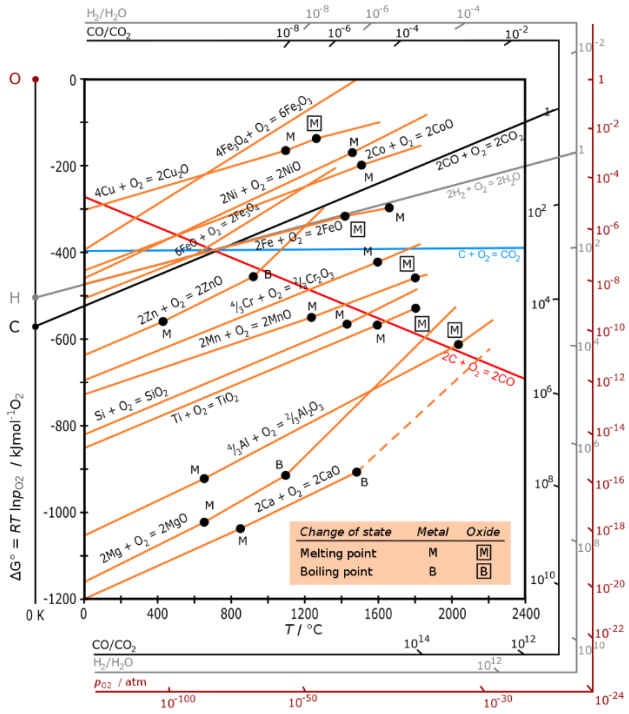

Figure 2.1 The Ellingham Diagram [10]

In Figure 2.1 the Ellingham Diagram is showcased, where the x-axis represents the temperature and the y-axis demonstrates the standard Gibbs free energy of oxidation reaction [9]. Furthermore, the linear line on the diagram describes how stable the oxides are as a function of temperature. This means that the lower the line is placed in the diagram, the more stable the oxide is and oppositely with less stable oxides. An example of this is chromia which is placed at the lower parts of the diagram. Chromia exhibits a low ΔG and therefore has a highly spontaneous formation, contributing to its stability. The diagram can also compare the oxidation rate when CO/CO_2 and H_2/H_2O ratios are active in different carbon oxides and water vapor mixture, along with partial pressure for oxygen [9].

2.2 Oxide formation

Oxidation of metals occurs when oxygen interacts with a metal surface (Fig. 2.2). Initially, oxygen is adsorbed on the metal surface leading to reduction of the oxygen molecule via

transferring electrons from the metal. [10]. The oxide will continue to grow laterally until the whole metal surface is covered. Later oxide growth is dependent on the diffusion rate of ionic species through the oxide scale [10].

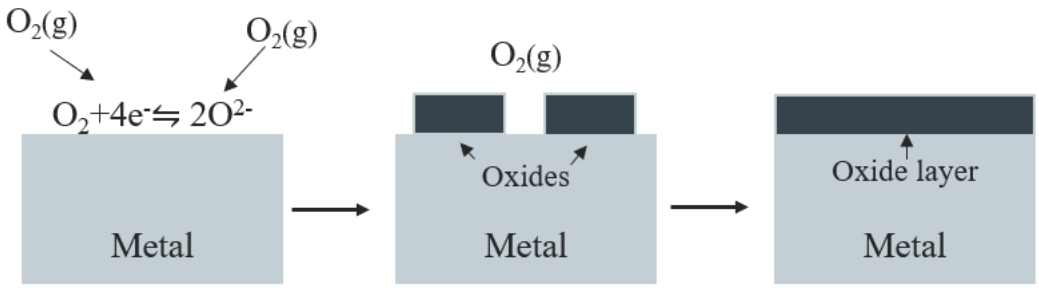

Figure 2.2 Illustration of an oxide formation

As the third and last step in Figure 2.2 above is demonstrating, the metal and the atmosphere doesn't have any direct contact with each other when the scale has formed throughout the whole surface. The oxide growth rate depends on various parameters such as temperature and defects in the oxide scale. [3,10,11].

Oxide knowledge is highly important when it comes to corrosion protection. An oxide can have numerous properties that promotes its protectiveness. These properties can have a slow growth rate, a strong adhesion with underlying material, a compact and continuous layer and a high melting point. Commonly observed oxides for high temperatures will be presented below [10]:

Hematite (Fe_2O_3): Hematite has the most protective properties of all iron-based oxides and has a good protection rate up to 500 °C in dry atmosphere [13].

Magnetite (Fe_3O_4): Magnetite is a less protective iron-based oxide than hematite. Under high oxygen pressure it commonly shows metal deficiency [3].

Wüstite ($Fe_{1-x}O$): Wüstite has severely worse protection properties than both magnetite and hematite due to its high ion diffusion rate. It usually forms from iron solids in temperature above 570 °C [13].

Alumina (Al_2O_3): As mentioned in the introduction, FeCrAl at temperatures above 900 °C forms a good protection oxide called α-Al_2O_3. However, in lower temperatures this alumina

phase is slow growing due to its thermodynamic instability and thus a less protective version called γ-Al_2O_3 is more observed [6].

Chromia (Cr_2O_3): The only stable chromium-based oxide at high temperatures is chromia showing a slow growth rate up to 1000 °C. Its corrosion protection succeeds all iron-rich oxides and is commonly formed on Ni-based alloys [3,6].

2.2.1 Kinetics

The Ellingham diagram described the stability of oxide formation for metals as a function of temperature. When discussing the kinetics of corrosion, it describes how the reaction rate can be influenced. Additionally, there can be several factors affecting the corrosion rate for instance metal pretreatment, temperature or time. Moreover, the kinetics of the oxidation can be calculated by quantifying the mass gain or loss for the metal over time [14].

The oxidation rate may for this reason be categorized into three different rate laws each one with described steps during oxide formation [14].

1. **Linear rate law**: In this condition, the corrosion rate is constant and having a thus self-sufficient consumption of the amount of metal or gas. For this reason, the oxide scale is not able to be protective [8].
2. **Logarithmic rate law**: The corrosion rate will start with a rapid growth rate at first, but the rate will start to decrease relatively quickly. This rate is mostly common in temperatures between 300 ℃-400 ℃ [8].
3. **Parabolic rate law**: This is the most common rate of oxidation in high temperatures. The oxidation rate will decrease due to an increase of the thickness of oxide scale leading to the diffusion of oxygen ions to reach the corrosion front takes longer time (or for metal ions to reach the gas environment [8].

These rate law can be described as a function for mass gain over time where the slope is the growth rate. Furthermore, the growth rate describes of many oxygen particles that can diffuse through oxide to react with the metal. In some cases, the forming oxide scale on the surface will be protective and slow growing. However, there are several ways to break this scale. It can break by itself by the gradual reduction of the material but also by other reasons, such as cracks formation. Upon destroying the protective oxide scale, a kinetic transition transpires which is

called breakaway corrosion [8]. For example, when an oxide with a parabolic growth abruptly transitions to a linear growth [8]. When looking at the presence of heavy metal chlorides, such as $PbCl_2$ which is highly reactive, breakaway corrosion have been commonly observed by $PbCl_2$ accelerating the corrosion rate breaking down the protective oxide scale. [3]

2.2 The influence of PbO and $PbCl_2$

Problems with lead (Pb) present in WtE systems have been discussed in several decades and several studies have shown that Pb compounds show an accelerated corrosion rate during combustion of waste material [3,6,15]. The explanation for this can be the high reactivity and leads ability to interact with the oxide scale, making the oxide break and dissolve. This results in breakaway corrosion where an uneven oxide scale is formed and therefore more ions can diffuse through the oxide and the corrosion attack can occur more rapidly.

In previous studies PbO have shown to not particularly accelerate the corrosion rate and oxide scale growth to both low-alloyed steel and austenitic steels [3, 15] At least comparing to $PbCl_2$ which has a highly aggressive localized impact on the acceleration of the corrosion rate. This is resulting in an uneven oxide where breakaway corrosion has a severely higher chance of happening due to its heterogenous surface. Therefore, studies have shown it to breakdown even protective oxide scales, such as Cr_2O_3, which are formed in Ni-based alloys [3,6, 13].

The main reason for $PbCl_2$ to be extremely aggressive is suggested to be the containing of Cl [3]. Chlorine is a highly reactive and volatile element and can therefore release and diffuses through the oxide and metal, thus contributing to the acceleration of the corrosion rate [3]. However, as of today the full mechanism behind $PbCl_2$ aggressive corrosion attacks is not fully understood.

2.3 SEM – Scanning Electron Microscopy

SEM is an electron microscopy that enables imaging of materials down to the nanometre scale and it is commonly used in the material science research [16]. The main difference between optical microscopy using light and SEM is that SEM is using an electron beam hitting the sample with high energy. Electrons have lower wavelengths, which results in finer details in the image than optical microscopy [16].

The electron beam generates from the electron gun in the top section of the instrument. This beam is usually generated in an energy range of a few hundred eV to 60 keV and the instrument is operated under vacuum conditions hindering the electrons from being disrupted by other particles. When the beam interacts with the sample, it produces a variety of signals which various detectors uses to obatin different information from the sample. These signals include backscattered electrons, (BSE), secondary electrons (SE) and x-rays [16].

2.4.1 The Main Difference between BSE and SE

Electrons generated from the electron gun will experience different elastic and inelastic scattering when interacting with the sample of interest.

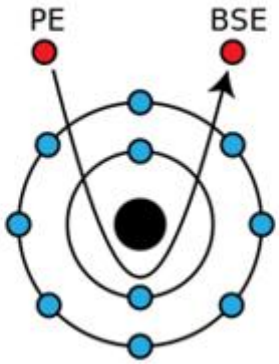

Figure 2.6: Sketch of Backscattered electron scattered through the atom. [16]

Figure 2.6 illustrates electrons scattering through an atom. The forces between the positive nucleus and the beam electrons are resulting in elastic scattering electrons. These electrons are scattered through all angles. When an electron is scattered through the atom at an angle greater than 90° it is called a backscattered electron (BSE). This is described in figure 2.6 above. Backscattered electrons constitute most of the electron signal and has a substantial ratio of the total energy from the electron beam. At the time when the scattered electron displaces from the atom and out to the vacuum, a detector obtains the information and creates a backscattered electron image [16].

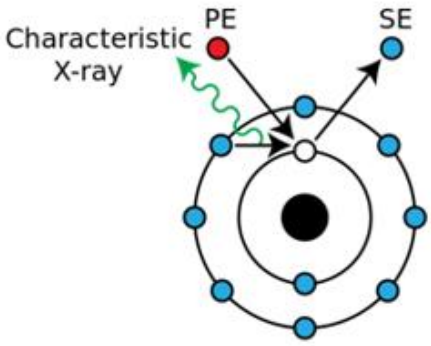

Figure 2.7: Sketch of secondary electron scattered through the atom. [17]

Furthermore, some electrons that the detector obtains are electrons which got ejected from the atom. These electrons are called secondary electrons (SE). When an incident electron impacts an electron of an atom, the electron of the atom is being knocked out from their shell. This is illustrated in figure 2.7. Secondary electrons have lower kinetic energy leading to reduced interaction volume caused by electrons only escaping to the top nanometre layer of the sample. This makes it possible to generate secondary electrons images [16].

The difference between these two types of images is the contrast where BSE's contrast is a compositional contrast and SE's is a topographic contrast. With compositional contrast the images become clearer when looking at different composition of materials. On the image the heavier compound becomes brighter than the lighter compound. With topographic contrast the difference is the surface height or topography of the sample [16].

2.4.2 EDX – Energy Dispersive X-ray

Energy Dispersive X-ray (EDX) is a technique that is usually coupled with the SEM instrument [18]. The instrument technique classify different composition in the sample can by using the primary electron beam. This is done by the primary electron beam colliding with the atom realising electrons from their inner shells. This makes the electron ejecting to an outer shell and thus transfer to an excited status. When the electron from the outer shell return to its originally state in the inner shells, it will then release in x-ray photons energy. With the energy from the photon being released, the instrument can classify the element. However, some elements release the same photon energy making EDX only an overall good compliment for BSE imaging [6,18].

2.4.3 BIB – Broad Ion-Beam

When performing analysis of cross section, the area must first be significant polished, such that mechanical polish is not enough. This can be done by using a broad ion-beam (BIB) instrument, resulting in being polished in nanometre level [19]. A BIB instrument can etch the sample with ions, usually argon-based ions, so the outer surface extracts. This is the result from energy transfers during the collision with the surface and the subsequent releasing of atoms [20].

3. Method and materials

In section 3, the experimental method will be represented. To evaluate the corrosion rate for both FeCrAl alloys and Ni-based alloys, the samples needed to be firstly prepared then exposed and lastly analysed. The sample preparation consisted of grinding, polishing and cleaning the samples. The exposure consisted of placing the samples in a benched furnace for 168 hours. Lastly the investigation included an analysis from SEM instrument. In this study the Ni-based alloy was already prepared for exposure and so FeCrAl was the only alloy being prepared. All reference data for the low alloyed steel refence came from Hampus Lindmark's licentiate thesis [3]. In Table 3.1 below the different chemical compositions are presented for the materials used in this study.

Table 3.1: Chemical composition of the materials in wt%.

	Fe	Cr	Al	Ni	Si	Mo	Mn
EF101	Bal	12.4	3,7	x	1,3	x	<0,1
625	4	21,5	x	61	0,2	8,7	0,15
T22	Bal	1,9-2,6	x	x	0,5	0,9-1,1	0,3-0,6

3.1 Sample preparation

The metal components with the dimensions 15 x 15 x 2 mm were firstly having its edges ground until a homogenous surface was achieved. This was done by mechanically grounding the surface with a silicon paper (SIC) having a grit size of 1000 and utilizing water as lubricant. Thereafter, the samples surfaces were grounded in water together with different SIC papers with grit size of 500, 1000, 2400 and 4000. To begin with the SIC paper with grit size of 500 was used in 40 seconds interval until the most severe scratches were grounded away. Afterwards the SIC paper with grit size 1000, 2400 and 4000 were used in 30-40 seconds intervals. Following that, the samples were polished until a mirror-like appearance with three different diamond suspensions of 9, 3 and 1 µm. The procedure was done on both sides of the samples. Lastly the samples were cleaned with acetone and thereafter submerged into different centrifuge tubes of 7 ml acetone during 15 minutes in an Elmasonic P ultrasonic bath.

Before exposure the samples were also needed to be sprayed with the heavy metal compounds, that being PbO or $PbCl_2$. This was achieved by spraying a 0.185 mg/cm^2 $PbCl_2$ deionized water

solution on each side. For the PbO a deionized water slurry was used instead. When the samples were sprayed, they were also weighed.

3.2 Exposure

After sample preparation, the samples were placed in an alumina sample holder and then placed in the furnace. Before that a couple of things needed to be done. The flow had to be measured and for that a flowmeter was used. The reason for this was because of the desire of having an atmosphere in the furnace tube that is calibrated to 20 % H_2O and a 5 % O_2 + N_2 balance (vol%). The temperature was measured to 400 ℃ ± 2 ℃ to have a temperature relevant for water wall application. The water vapor was connected to a water bath set to 60 ℃. This was done to obtain a vapor pressure of water that represents a humidity of 20 vol. % in the gas. Because of this it was necessary to add more water every day to the bath. The exposure time for all experiments was 168 hours, with other words one week. In table 3.2 below different exact values of the different parameters during the exposure process is presented.

Table 3.2: Temperature and flows during exposure.

Exposures	Airflow (ml/min)	N_2 -flow (ml/min)	Temperature °C
EF101 with PbO	732	1730	400
625 with PbO	732	1726	400
EF101 with $PbCl_2$	732	1726	400

3.3 Analysis

After the exposure a plan view analysis was carried out using SEM/EDX. The first method being applied to the sample with SEM and EDX instrument. The X-ray instrument utilized was an Oxford Ince energy detector coupled with the SEM and EDX analyse instrument. The accelerated electron voltage for SEM instrument was set to 15-20 KeV. Backscattered electrons (BSE) detector as well as secondary electrons (SE) detector were both used for the analysis of the plan view. An EDX analysis in the form of point and map analysis were carried out at 20 KeV.

Second part of the analysis was a cross sections analysis being performed identical to the plan view with both SEM and EDX instruments. However, before the analysis the samples were

sputter coated with gold. The reason being to increase the contrast and the conductivity of the material to avoid charging effect during SEM. Thereafter a silicon wafer was glued on top of the sample. The glue was a Loctite 415, and the sample was left to dry overnight. Finally, the sample was cut using a Struers TXP instrument applying 2100 rpm. Subsequently, the samples were ion milled for 6 hours with an accelerated voltage of 8 KV. Subsequently, the cross sections were analysed using SEM and EDX.

4.Results

In this section the result from the three exposures will be presented as well as results from the analytical instruments. Furthermore, all images and diagrams will be presented in this section.

4.1 Plan view analysis

Plan view analysis was first observing the EF101 and 625 exposed to PbO and thereafter EF101 exposed to $PbCl_2$. All samples were used by SEM and BSE images and EDX analysis as main methods.

4.1.1 EF101 exposed to PbO

First exposure was EF101 with PbO where the following BSE images below illustrates different area of the FeCrAl sample which has been exposed during 168 hours:

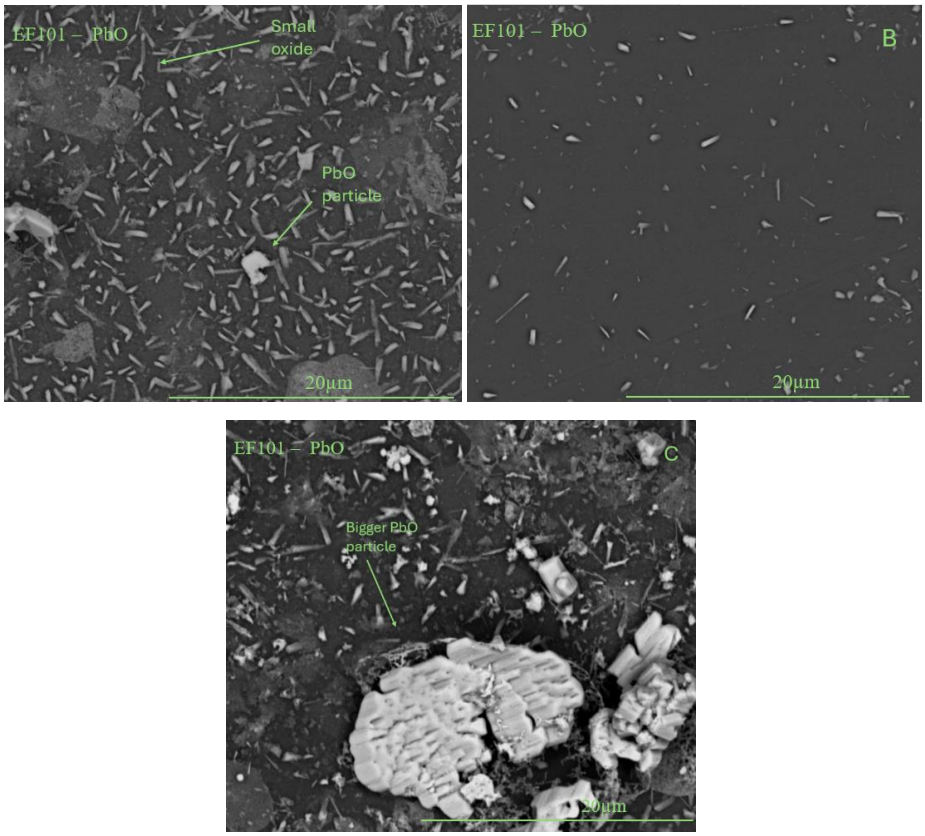

Figure 4.1: Image A, B and C all showing different areas of the same sample taken with BSE.

Figure 4.1 shows three different areas of the same sample with the same magnification and electron beam energy, being 8000x and 15 keV. The images are not showing any kind of oxide scale, apart from picture A that seems to have a small start of an oxide. The difference between these pictures is the amount of white particles on the sample. The white particles are suggested to be sprayed PbO because of its heavier compound being brighter on BSE images. BSE image A depicting smaller shards of PbO and start of an oxidation in both left and right corner. However, BSE image B is from an area of the sample where limited PbO have been sprayed. In BSE image C a bigger particle of PbO is showing although no oxidation has started. The darker area of all images is probably the alloy which contains a lot of iron, chromium and aluminium.

With EDX analysis, BSE image C from figure 4.1 was mainly analysed because of the variety of different particles in this image. Only spectrum 2, 4, 5 and 6 will be in focus and their placements are shown in figure 4.2 below.

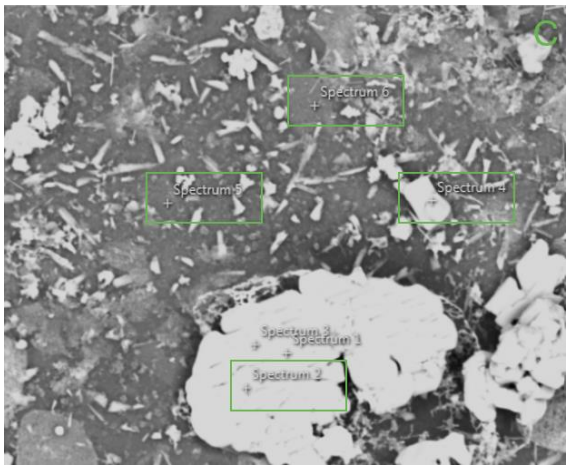

Figure 4.2: BSE image of where the different spectrum was selected.

As showcased in figure 4.2, Spectrums 2 and 4 were selected where the brighter area is, assumably PbO particles and spectrum 5 and 6 is selected in the darker area, probably the iron-based alloy. From these spectrum points the atomic percentage was calculated by help of EDX. This is presented in table 4.2 below:

Table 4.1: Table of atomic percentage for different elements for EDX analysis EF101 exposed to PbO.

Spectrum	O (%)	Fe (%)	Cr (%)	Al (%)	Pb (%)	Si (%)
2	51	6	1	0	40	0
4	44	18	4	1	33	1
5	18	58	11	5	5	3
6	14	65	11	6	2	2

From Table 4.1 it is noted that Pb and oxygen are the most dominated elements in spectrum 2 and 4 with 51 % and 44 % oxygen and 40 % respectively 33% lead. By its stoichiometry it could be both PbO or Pb_3O_4 and no conclusion can be made. Additionally, from point 5 and 6 it appears that Fe is around 60 %, Cr is around 11 % and Al around 5-6 %.

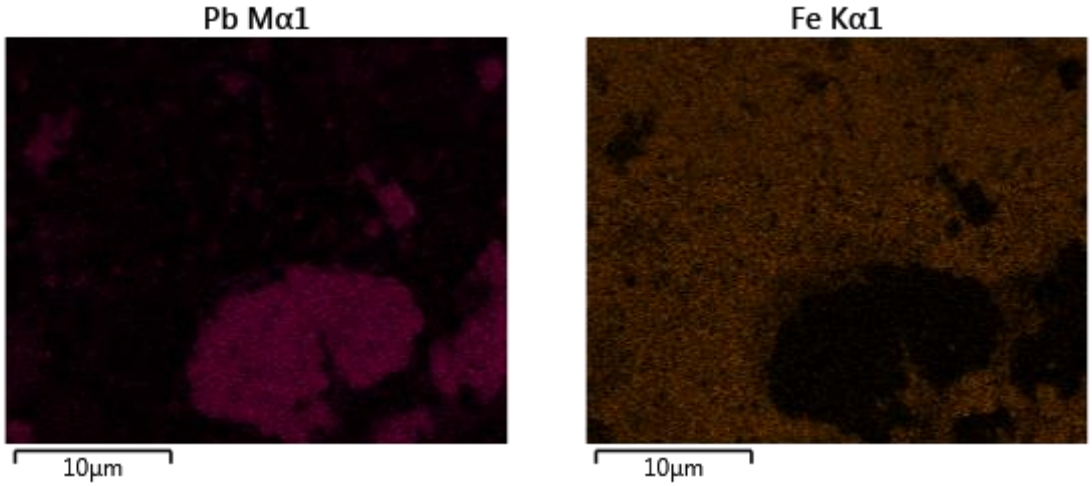

Figure 4.3: Map analysing of picture C from figure 4.1, where mapping element Pb is to the left and right is iron.

From Figure 4.3 it is observed that Pb highlights in pink and Fe in orange. Iron is widely detected over the image except the big brighter particle where Pb is detected.

4.1.2 625 exposed to PbO

The Ni-based 625 alloy will be referred and analysed to compare it with EF101 exposed to PbO.

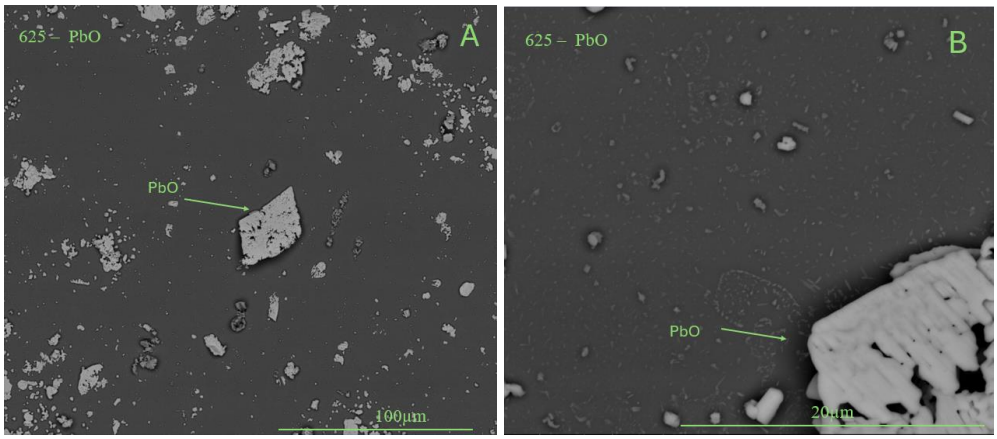

Figure 4.4: BSE Images of different sites for 625 alloy exposed to PbO. A has magnification 1000x, B has 8000x.

Figure 4.4 shows it two different magnifications where BSE image A is observing a greater area of the surface. With the magnification at 1000x, the notation of many different sprayed PbO particles can be spotted. On the other hand, the sample surface is homogenous. The BSE image B, show a surface covered small particles. If compared to the particles of EF101 with magnification at 8000x, this surface implies to have a more homogenous surface.

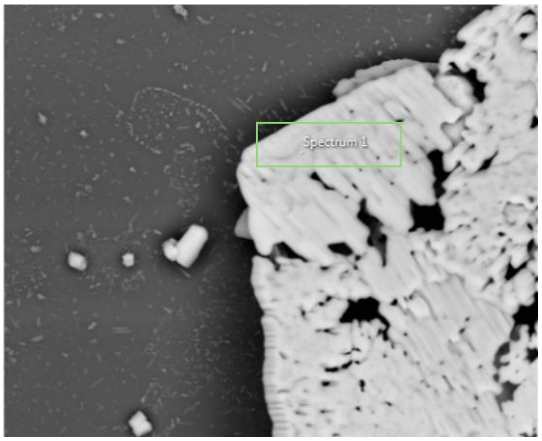

Figure 4.5: Showing two different selected spectrums named Spectrum 1.

Spectrum 1 was marked at the supposedly big PbO particles. For verify this the EDX analysis was conducted.

Table 4.2: Table of atomic percentage elements for EDX analysis. 625 exposed to PbO.

	O (%)	Mo (%)	Cr (%)	Fe (%)	Ni (%)	Pb (%)
Spectrum 1	53	0	2	0	7	37

Table 4.2 showcases the composition of the Pb particle. This particle has the same atomic percentage as similar points in Table 4.1 with 37 % Pb and 53 % O. Furthermore, for clarification of Ni detection, a mapping of the area was accomplished as well with EDX.

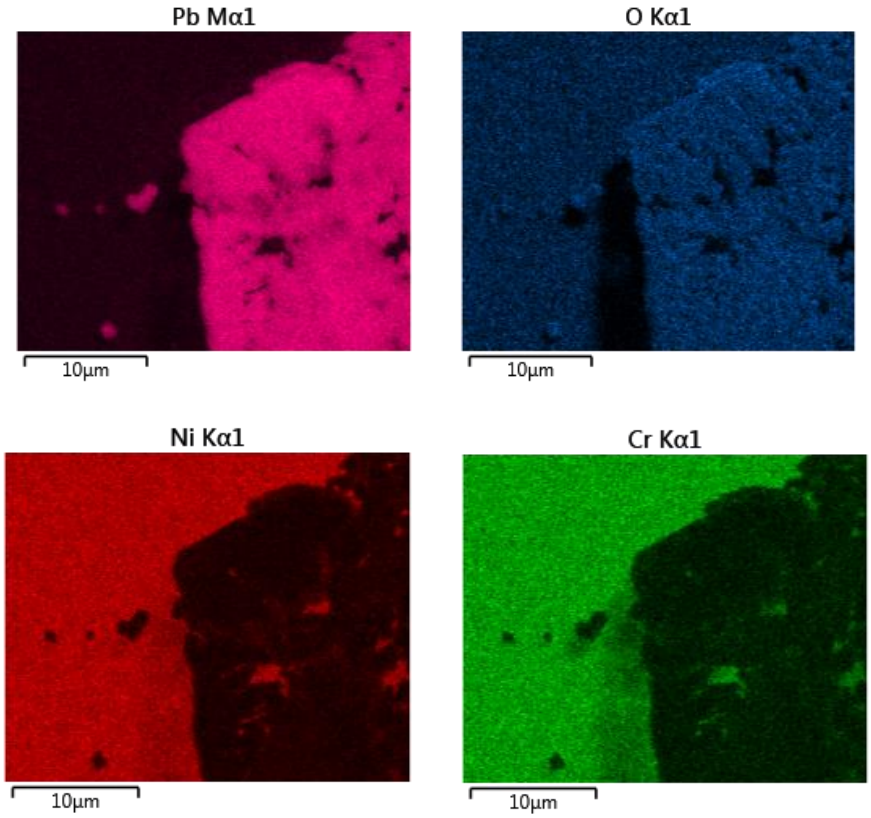

Figure 4.6: Detection of elements with EDX mapping, Top left is Pb Map, Top right is O map, bottom left is Ni Map and bottom right is Cr Map.

Figure 4.6 portrays four different maps where different elements have been detected. In top left the Pb map is displayed, and the big white particle contains a high degree of Pb. For oxygen in top right corner of the figure it is detected all over the image. However, the oxygen concentration is higher in the PbO particle.

4.1.3 EF101 exposed to $PbCl_2$.

EF101 was exposed in the presence of $PbCl_2$ in order to compare it with PbO and investigate the impact of chlorine. From the BSE images the following images were observed:

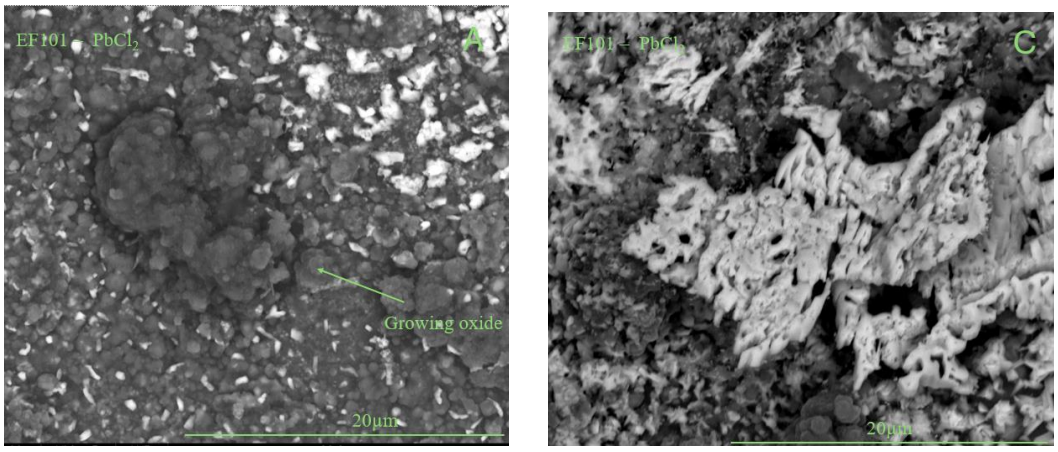

Figure 4.7: Two BSE images of EF101 sample exposed to $PbCl_2$ for 168 hours, both images A and B was taken on the same sample. A is the image on the left and B right.

In figure 4.7 above, two different oxidized areas are observed. Both BSE images have the same magnification of 8000x and are from the same sample. However, the contrast for the two pictures is different. Furthermore, the two images seem to have grown oxides although these oxides are different. BSE image A showing a darker compound meaning that the compound is lighter than BSE image B that showing a brighter compound. For further classification an EDX analysis was conducted.

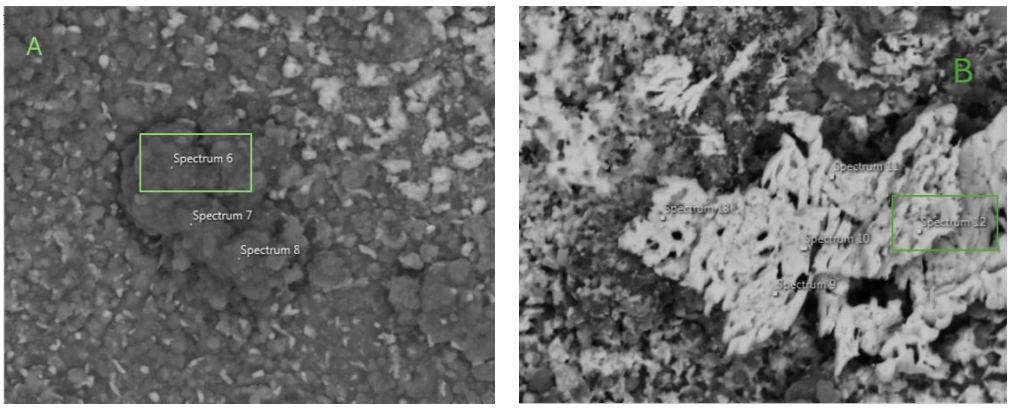

Figure 4.8: Showing the position of the two spectrums chosen to do the EDX analysis.

In figure 4.8 the two spectrums selected where the following analysis is showcased. In image A, taken from figure 4.7, the point is Spectrum 6 placed on the top of the bigger oxide. In image B, Spectrum 12 is on the right side of the image. For verifying the composition, the atomic percentage was calculated additionally.

Table 4.3: Atomic percentage of Spectrum 6 and 12.

Points	Pb (%)	Fe (%)	O (%)	Cr (%)	Cl (%)	Al (%)
Spectrum 6	1	34	61	3	0	1
Spectrum 12	37	8	53	1	0	0

In table 4.3 three observations can be noted. Firstly, the atomic composition for Spectrum 6 where iron and oxygen have 34 % and 61 % atomic percent respectively. This is different from when EF101 was exposed to PbO (Table 4.1) where Fe was the most dominated element, thus the metal has been oxidized. Secondly, spectrum 12 has a composition for Pb and oxygen of 37 % and 53 % which is almost the same for when EF101 was exposed to PbO, showcasing that it oxidized to the same species in both experiments. Lastly, Cl in both points is barely or to no extent detected. More comprehensive analysis of this phenomenon will be discussed in the discussion section.

Final observation will be to compare EF101 exposed to both PbO and $PbCl_2$ with a lower magnification, with other words an image examining a bigger portion of the two samples.

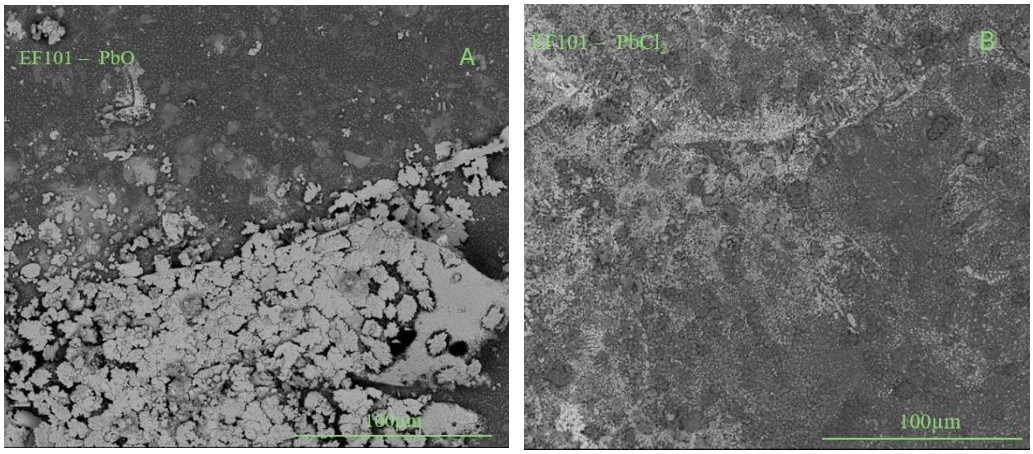

Figure 4.9: BSE image A is EF101 exposed to PbO and image B is EF101 exposed to $PbCl_2$ with magnification 1000x.

These images can be a bit misleading as BSE image A is showcasing a big group of PbO particles covering half of the image. However, when observing only the sample's surface it can be acknowledge that image A is more homogenous than BSE image B. The reason for this is that in image B several smaller growing oxides are spotted while on BSE image A only small particles of PbO are observed.

4.2 Cross-section analysis

Moreover, to the second section the cross-section analysis will be presented. The samples here are the same samples as in the plan view samples and under equal exposure conditions. Unfortunately, the Ni-based sample was unevenly cut and therefore only the two EF101 samples will be analysed. Thus, the main objective in this section will be to describe the influence of chlorine to the samples.

4.2.1 Cross-section of EF101 exposed to PbO

The same method was applied as in the plan view analysis by using the SEM instrument for taking BSE images. Thereafter followed an analysis with EDX instrument either with a point or with a map function.

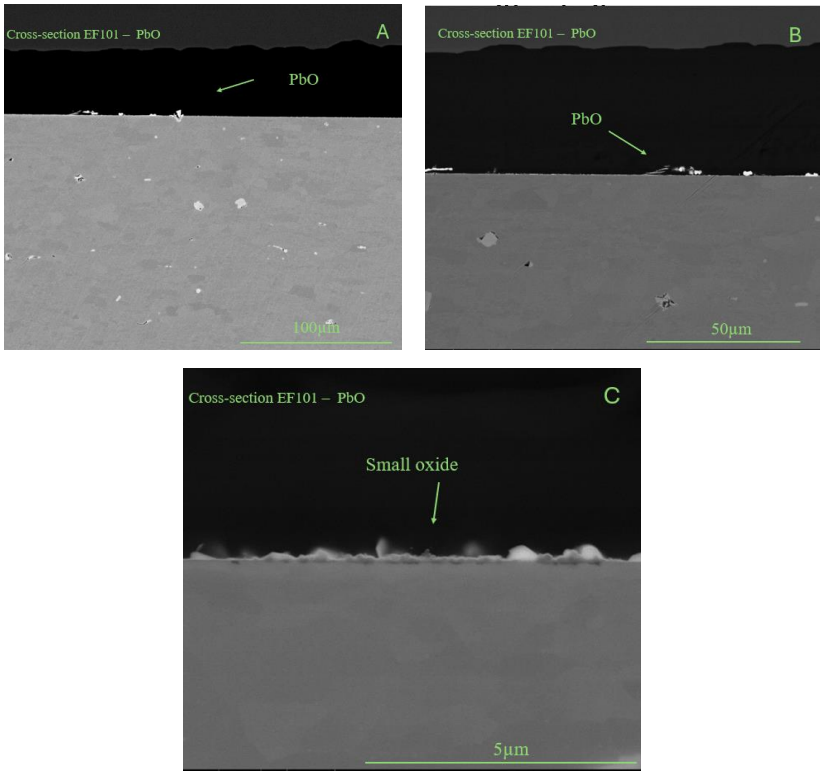

Figure 4.10 Three cross section images with different magnification when EF101 is exposed to PbO for 168 hours at 400 C°.

Figure 4.10 consists of three different images. Top right image is BSE image A where the magnification is at 1000x and therefore a greater area of the sample is being observed. The surface is mostly homogenous with a few PbO particles. In the top left is BSE image B showing a magnification at 2000x similarly to image A. A homogeneous surface with a handful of PbO

shards can be observed. Finally, BSE image C at the bottom has a magnification at 30000x, analysing the sample up close. Here a minor oxide layer is spotted through the surface, however this layer is thin. EDX detection was conducted for analysing the oxide scale. Because of the scale being so thin the magnification needed to be increased for the selections of spectrums.

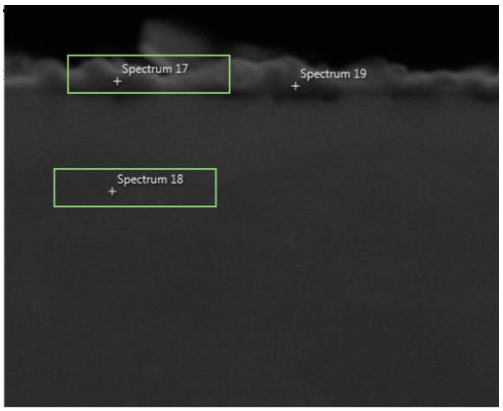

Figure 4.11: Zoomed in BSE image of picture C in Figure 4.14 with magnification at 60000x. Showing EDX analysis of spectrum 17 and 18.

Figure 4.11 shows the place of the two spectrums that will be EDX analysed. Spectrum 17 is located within the small oxide scale and spectrum 18 is selected in the alloy complex. This is demonstrating whether there is any difference and therefore displaying any oxide growth. For confirmation the atomic percentage was calculated.

Table 4.4: Atomic percentage of Spectrum 17 and Spectrum 18 from figure 4.15

	Fe (%)	O (%)	Cr (%)	Al (%)	Pb (%)	Si (%)
Spectrum 17	44	41	6	5	2	2
Spectrum 18	75	2	12	8	0	3

Table 4.4 confirms that there is a major difference between the two spectrums looking at iron, oxygen and chromium percentages. Where iron and chromium noticeably have decreased with having only 31 % and 6 % on the surface compared to its inner parts. Nevertheless, oxygen has substantially increased at the surface by 39 %. This underscore that the surface has a small oxide growth. Finally, from the table 4.4 both spectrums have limited amount of Pb.

4.2.2 Cross-section of EF101 exposed to $PbCl_2$.

Identical procedure was conducted when analysing a cross-section of a EF101 sample exposed to $PbCl_2$. The BSE images taken from SEM has equal magnification to evaluate if there are any variation.

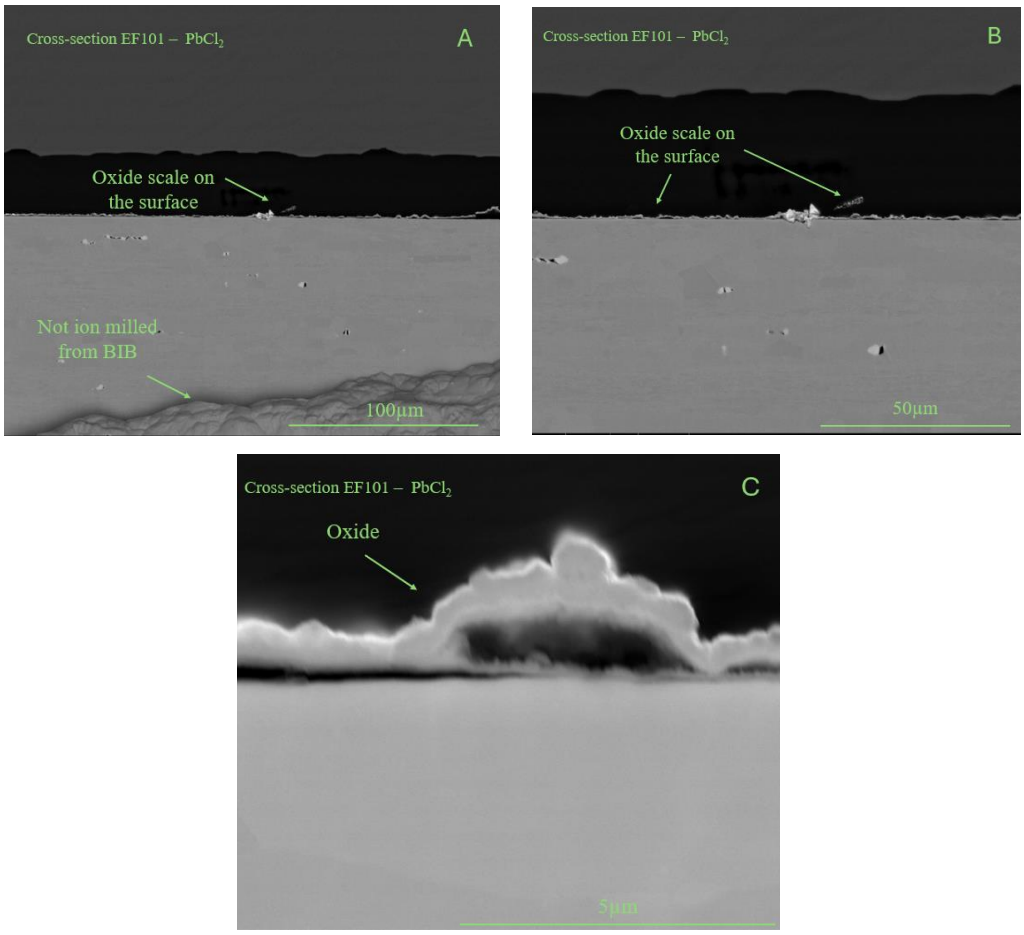

Figure 4.12: Three cross section BSE images with different magnification when EF101 is exposed to $PbCl_2$ for 168 hours at 400 °C.

The three pictures in figure 4.12 displays a substantial larger oxide scale and growth. In comparison with picture A in figure 4.10, BSE image A here has a more heterogeneous surface, and the oxide scale is visible from a magnification at 1000x. When the magnification is increased (image C) the oxide indicates having an outward growing layer. For classification of which oxide, an EDX analysis was conducted.

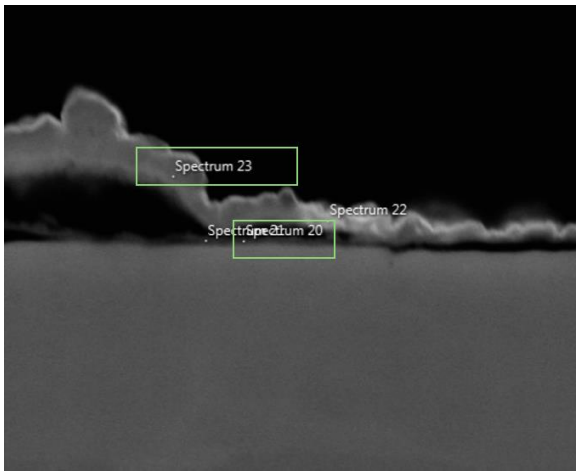

Figure 4.13: Image showing a growing oxide with Spectrum 20 and Spectrum 23 has points doing the analysis.

Chosen area where the analysis was conducted is showcased in figure 4.13 where the focus will be on Spectrum 20 and 23 which are framed on the image. Spectrum 20 is at the surface and 23 is in the outward growing oxide. The following atomic percentages are presented:

Table 4.5: Atomic percentage for Spectrum 20 and 23.

	Fe (%)	O (%)	Cr (%)	Al (%)	Pb (%)	Cl (%)
Spectrum 20	54	31	8	3	1	1
Spectrum 23	39	55	3	1	1	0

From table 4.5 where the atomic percentage is calculated there is a notably difference between the two selected points. The surface is containing a considerable amount of oxygen with 31 % but the main element is still iron with 54 %. However, at the outgrowing oxide layer the oxygen has increased to 55 % and all components for FeCrAl alloy have decreased, hence an oxide has formed. With the high amount of both iron and oxygen it is presumably an iron-rich oxide. Lastly, the detection of chlorine is minimum in this analysis as well, confirming that it is diffused somewhere.

For summarising both exposure with $PbCl_2$, the oxide growth on these samples have been limited. For a reference, an image illustrating $PbCl_2$ exposure for low-alloy steel T22 will be presented:

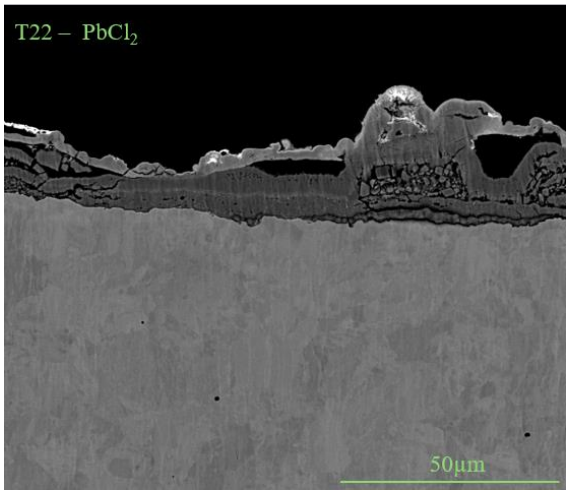

Figure 4.14: Image of low alloy steel exposed to $PbCl_2$ for 168 hours, adempted from [3].

Image showed in figure 4.14 has a magnification at 2000x and the material is low alloyed steel T22 exposed with $PbCl_2$ a duration of 168 hours. The oxidation rate is significantly more evident and the homogenous surface seeing in EF101 cross-section samples has completely vanished in figure 4.16. Furthermore, different oxides have started to grow, presumably oxides which are Pb-based, and iron based.

4.2.3 Oxide growth

The final analysis involved the measuring of the oxide thickness. This was done by using the scale from the images and convert the length to pixels using the program Inskcape. First, the number of pixels equivalent to 5 µm was measured. Furthermore, the number of pixels representing the oxide layer was measured and the percentage of the oxide layer was then determined by dividing pixels of the oxide layer with pixels corresponding to 5 µm. Lastly, this percentage was multiplied by 5 µm to determine the thickness of the oxide layer in micrometres. Seven different points from the picture was measured and then the mean value from these points were calculated.

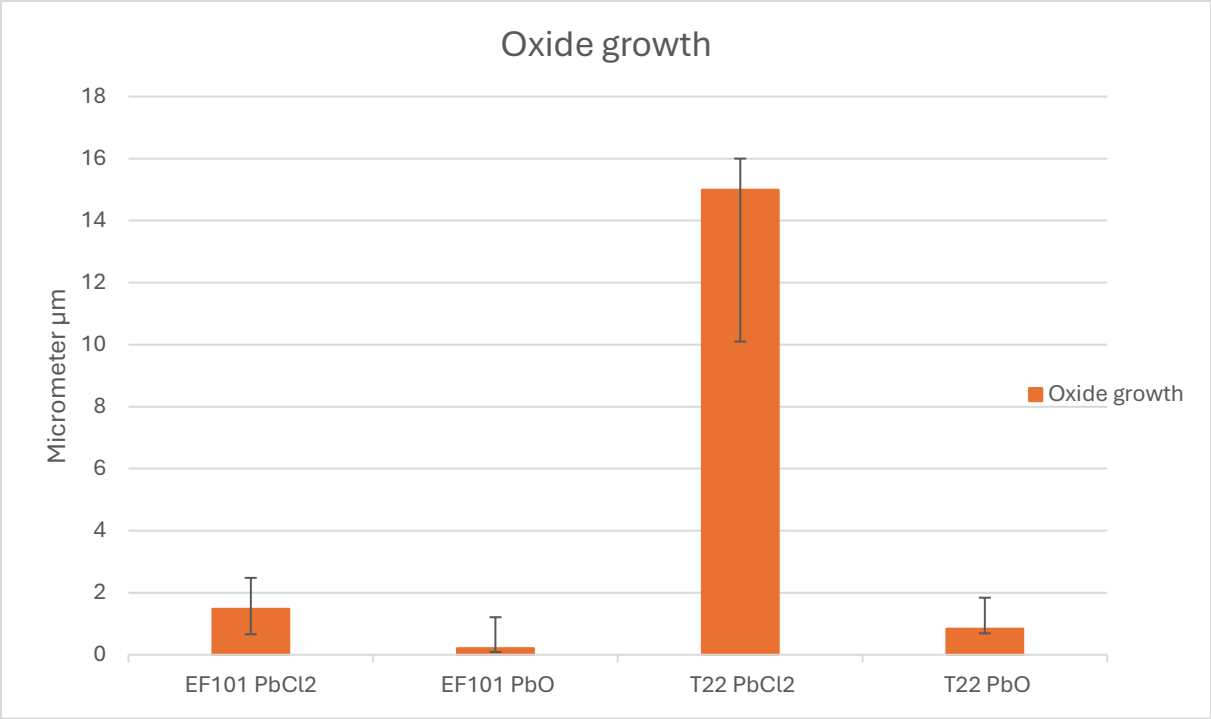

Diagram 4.1: Oxide growth for EF101 exposed to $PbCl_2$ and PbO with references and standard deviations."

In diagram 4.1 the oxide thickness results are presented for EF101 exposed for $PbCl_2$ and PbO with two references being low alloyed steel exposed to the same lean compounds. The results indicates primarily that EF101 is significantly protective against corrosion compared to low alloy steel. The mean value for the alloys when exposed to $PbCl_2$ was 1.48 µm for EF101 and 15 µm for low alloy steel. When exposed to PbO the thickness was 0.21 µm for EF101 and 0.84 µm. This means that there is a greater difference when $PbCl_2$ exists in the environment than when PbO is present. Finally, the four staples in the middle of the oxide thickness stables are the standard deviation from the four different measurements, calculated by standard deviation function. They represent the variation of the data for the different points selected at the sample. The highest standard deviation was low alloyed steel exposed to $PbCl_2$ with 4.9 and the lowest was EF101 exposed to PbO with 0.21.

5.Discussion and Conclusion

The aim for this project was to evaluate the corrosion rate for the newly developed FeCrAl alloy EF101 in an environment simulating the water-wall of waste fired boiler. Furthermore, EF101 was compared the Ni-based alloy 625 and the low-alloyed steel T22. After exposure, the samples were analysed using SEM and EDX in order to quantify the oxide growth. From SEM several BSE and SE images were taken for both classifying the composition of the samples and to observe the morphology of the sample. All images used in the results section were used with BSE due to the non-significant oxide growth of the sample and the focus became more of analysing and classifying the different compound compositions.

From the results it can be observed that EF101 have significantly greater corrosion protection if compared to the reference low-alloyed steel T22. When exposed to PbO the EF101 alloy has very limited oxide growth. The is shown in Diagram 4.1 where the average oxide growth was only 0.21 μm. This is even confirmed by both cross-sectional and plan view images. The EDX analysis also indicates that the sample have not been oxidized at a significant rate.

Furthermore, compared to the Ni-based alloy 625 the results for EF101 shows equal good protection properties for corrosion. There is a slight difference observed at the surface of the sample, where the Ni-based alloy obtains a more homogenous oxide surface. The difference is not significant, and the exposure time was 1 week hence the difference can be much greater in for longer exposure times. However, the cross-section of alloy 625 could not be analysed and it is suggested to perform this analysis in the future in order to gain more knowledge about the corrosion attack.

The analysis of the $PbCl_2$ exposed samples showed a significant difference in oxide formation compared to the PbO exposed samples. The plan view image from SEM showcases a remarkable more heterogeneous surface and several smaller oxides are observed for EF101. EDX also shows that the oxide being formed is mainly iron-rich oxide (Table 4.5). The

explanation for this can be because of the protective oxides has broken and more unstable oxides has started to grow.

However, if compared to the reference low alloy steel the oxide formation is substantial lower. This is observed in Diagram 4.1 where the oxide thickness is measured and EF101 had an average thickness of 1.8 µm compared to low alloy steels having a thickness of 15 µm. This showcases that EF101 has a good protection against corrosion.

The EDX results showed no or very little amount of chlorine. It was only in Spectrum 20, Table 4.3, where chlorine was detected in small amounts, indicating that some of the chlorine has diffused through the oxide and down to the alloy/oxide interface. One reason for very little chlorine was detected is that chlorine has evaporated during the exposure because of its volatility properties.

In this study there is no major source of error that could have affected the results. However, there is still chance that different contaminations could have occurred or there could have been errors in measuring the flow or temperature before exposure. The major concern in this study was the limitation of time and the exposures being finished in time. Especially with Ni-based alloy where one exposure with $PbCl_2$ did not finish in time and the cross-section analysis with PbO was unsuccessful due to problems with the instrument.

Therefore, in future studies the focus should be on performing more exposure with EF101 and alloy 625 with $PbCl_2$. Several exposures must be accomplished so more data can be presented and be compared with the two alloys. Also expand the experimental parameters; in the water wall region of waste fired boiler many reactive compounds are present. One of these is hydrochloric acid. This comparison is of importance high since EF101 can be a potential sustainable substitute for the expensive Ni-based alloy.

As a conclusion, the EF101 has a protective rate against corrosion from heavy metal compounds. Especially when compared to the low alloy steel where the corrosion attack is significantly higher. The effect of chlorine in these corrosion environments was observed in this study. When compared with PbO, $PbCl_2$ was remarkably more aggressive in attacking the alloy. Due to limited results from the Ni-based alloy any conclusion of EF101 being a good candidate cannot be done in this study. In future studies the focus on the comparison between

EF101 and alloy 625 is important in order to increase the knowledge of protectiveness of these materials. This is critical for accomplishing a sustainable future and achieve Europe Commission's WtE goals.

Bibliography

[1]Zajemska M, Korombel A, Ławińska O. Risk factors for poland to achieve the european commission's recycling and landfill targets and their effects on waste-to-energy conversion: a review. Energies [Internet]. januari 2024. Available at: https://www.mdpi.com/1996-1073/17/5/1171

[2]Correddu F, Lunesu MF, Caratzu MF, Pulina G. Recalculating the global warming impact of italian livestock methane emissions with new metrics. Italian Journal of Animal Science [Internet]. 31 december 2023. Available at: https://www.tandfonline.com/doi/full/10.1080/1828051X.2023.2167616

[3] Lindmark H. High Temperature Corrosion in Wasted Fired Boilers: Insights into material selection for fluidized bed heat exchangers and the corrosivity of PbCl2 [Internet]. Chalmers; 2023. Available at: https://research.chalmers.se/publication/537752/file/537752_Fulltext.pdf

[4] Lindmark H, Jonsson T, Liske J. A time-resolved study of PbCl2-induced corrosion of low-alloyed steel in the presence of water vapour at 400 ◦C. Elsevier Ltd [Internet]. 09 january 2024; Available at: https://research.chalmers.se/publication/539863/file/539863_Fulltext.pdf

[5] Singh JB. Alloy 625: microstructure, properties and performance [Internet]. Singapore: Springer Nature Singapore; 2022. (Materials Horizons: From Nature to Nanomaterials). Available at: https://link.springer.com/10.1007/978-981-19-1562-8

[6] Eklund J. High Temperature Corrosion of FeCrAl Alloys in Biomass- and Wastefired Boilers [Internet]. Chalmers; 2020. Available at: https://research.chalmers.se/publication/521876/file/521876_Fulltext.pdf

[7] Sarrazin P. Mechanisms of High Temperature Corrosion [Internet]. Zurich Trans Tech Publications, Limited, 2008.; 2008. Available at: https://ebookcentral.proquest.com/lib/chalmers/reader.action?docID=1865165

[8] Jayanth Reddy M. Metallic materials for solid oxide fuel cells and electrolysers [Internet]. Chalmers; 2023. Available at: https://research.chalmers.se/publication/535305/file/535305_Fulltext.pdf

[9] Gialanella S, Malandruccolo A. Corrosion. I: Aerospace Alloys [Internet]. Cham: Springer International Publishing; 2020. Available at: https://doi.org/10.1007/978-3-030-24440-8_8

[10] Ellingham diagram. I: Wikipedia [Internet]. 2023. Available at: https://en.wikipedia.org/w/index.php?title=Ellingham_diagram&oldid=1171691259

[11] Phother-Simon J. High Temperature Corrosion of Superheaters in Biomass- and Waste-Fired Boilers: Combat on two fronts [Internet]. Chalmers; 2019. Available at: https://research.chalmers.se/publication/507819/file/507819_Fulltext.pdf

[12] Phother S. High-Temperature Corrosion Behavior in Biomass- and Waste-Fired Boilers [Internet]. Chalmers; 2020. Available at: https://research.chalmers.se/publication/518720/file/518720_Fulltext.pdf

[13] Larsson E. The Corrosive Effect of Chlorine Containing Species on Waterwalls and Superheater Materials in Waste and Biomass-Fired Power Plants [Internet]. Chalmers; 2016. Available at: https://publications.lib.chalmers.se/records/fulltext/246773/246773.pdf

[14] Alnegren P. Corrosion of Ferritic Stainless Steel Interconnects for Solid Oxide Cells – Challenging Operating Conditions [Internet]. Chalmers; 2018. Available at: https://research.chalmers.se/publication/503125/file/503125_Fulltext.pdf?fbclid=IwZXh0bgNhZW0CMTAAAR3sTvmU7zWxsvGaJelMn5TmIfES67Ie3oW8O3lHvUX_nJ3RmXA6ALOHm9M_aem_AbLzDs1x9zeurNdxbOtHT4L-yjjo_F6v3QBHemAVeG6WaXK_j6N8QGatHnU7A2SfErMzE3vXxsp_pHfEH-YGv6yS

[15] Bankiewicz D, Enestam S, Yrjas P, Hupa M. Experimental studies of Zn and Pb induced high temperature corrosion of two commercial boiler steels. Elsevier BV [Internet]. 11 januari 2012. Available at: https://www.sciencedirect.com/science/article/pii/S0378382011004346/pdfft?isDTMRedir=true

[16] Ul-Hamid A. A beginners' guide to scanning electron microscopy [Internet]. 1s Edition. Springer Cham; 2018. Available at: https://link.springer.com/book/10.1007/978-3-319-98482-7

[17] Scanning electron microscope. I: Wikipedia [Internet]. Available at: https://en.wikipedia.org/w/index.php?title=Scanning_electron_microscope&oldid=1224583063

[18] Ramohlola KE, Iwuoha EI, Hato MJ, Modibane KD. Instrumental Techniques for Characterization of Molybdenum Disulphide Nanostructures. Hindawi [Internet]. 2020; Available at: https://downloads.hindawi.com/journals/jamc/2020/8896698.pdf

[19] Gholinia A, Curd ME, Bousser E, Taylor K, Hosman T, Coyle S, m.fl. Coupled Broad Ion Beam–Scanning Electron Microscopy (Bib–sem) for polishing and three dimensional (3d) serial section tomography (Sst). Ultramicroscopy [Internet]. 01 juli 2020. Available at: https://www.sciencedirect.com/science/article/pii/S0304399119302098

[2] Desbois G, Urai JL, Kukla PA, Konstanty J, Baerle C. High-resolution 3D fabric and porosity model in a tight gas sandstone reservoir: A new approach to investigate microstructures from mm- to nm-scale combining argon beam cross-sectioning and SEM imaging. Elsevier BV [Internet]. 15 juni 2011. Available at: https://www.sciencedirect.com/science/article/pii/S0920410511001306/pdfft?isDTMRedir=true

Appendix

CHALMERS